Progress in Additive Manufacturing (2022) 7:609–626
https://doi.org/10.1007/s40964-021-00250-x

REVIEW ARTICLE

Metal FDM, a new extrusion-based additive manufacturing technology for manufacturing of metallic parts: a review

Haidar Ramazani[1] · **Abdolvahed Kami**[1]

Received: 1 August 2021 / Accepted: 4 December 2021 / Published online: 22 January 2022
© The Author(s), under exclusive licence to Springer Nature Switzerland AG 2021

Abstract
Recently, various additive manufacturing (AM) methods with a wide range of capabilities have been employed to produce metallic objects. Metals are a popular choice among AM materials due to their superior properties, despite being more challenging to print. Reduced product cost, the possibility for quick production and prototyping, and the capability of a produced component by high accuracy in a broad variety of shapes, geometrical complexity, size, and material are all advantages of metal AM technology. Metal fused deposition modeling (metal FDM) is a relatively new technique based on the widely used FDM process. It is a relatively low-cost competitor to other metal AM techniques such as selective laser melting (SLM). This review paper has explored the most recently issued publications in this extrusion-based metal additive manufacturing (EAM) technique. The main parameters in feedstock preparation, deposition and 3D printing, debinding, and sintering phases of the metal FDM process will be discussed and their influence on the mechanical and microstructural characteristics of the 3D-printed parts. Furthermore, the application of finite element modeling for metal FDM process analysis is explored. Finally, the challenges and gaps in the manufacturing of components and obtaining desired characteristics have been presented.

Keywords Additive manufacturing · 3D printing · Fused deposition modeling · Metal FDM · Extrusion-based AM

Abbreviations

ADAM	Atomic diffusion additive manufacturing
AM	Additive manufacturing
BJ	Binder jetting
BMD	Bound metal deposition
DIW	Direct ink writing
EAM	Extrusion-based additive manufacturing
EBM	Electron beam melting
FDM	Fused deposition modeling
FDMet	Fused deposition of metals
FEM	Finite element modeling
FFF	Fused filament fabrication
MF3	Metal fused filament fabrication
MIM	Metal Injection Molding
RWL	Restaurant waste lipids
SSMED	Semi-solid metal extrusion and deposition
SDS	Shaping, debinding & sintering
SLM	Selective laser melting
SLS	Selective laser sintering
SS	Stainless steel
TPE	Thermoplastic elastomer

✉ Abdolvahed Kami
akami@semnan.ac.ir

[1] Faculty of Mechanical Engineering, Semnan University, Semnan, Iran

1 Introduction

The term additive manufacturing (AM) refers to "the process of joining materials to make parts from 3D model data, usually layer upon layer, as opposed to subtractive and formative manufacturing methodologies" [1]. AM can manufacture geometrically complicated components in a short amount of time with relatively low tooling costs [2] and without material waste or the usage of molds. Vat photopolymerization, material extrusion, material jetting, binder jetting, sheet lamination, direct energy deposition, and powder bed fusion are the seven fundamental categories for AM technology specified by the ISO/ASTM standard [1].

Metals are one of the most widely used materials in AM, and metal AM technology has been studied for almost two decades [3]. On the other hand, Metal AM has its own set of difficulties and significant distinctions from commercial 3D printing of polymeric materials [4]. Powder bed fusion (including selective laser melting (SLM), selective laser sintering (SLS), direct metal laser sintering (DMLS), and

electron beam melting (EBM) [1]), material/binder jetting [5], and direct energy deposition (DED) are the most widely utilized metal AM techniques. These techniques are depicted in Fig. 1. SLM is currently well-established for industrial applications, but it comes at a significant expense in terms of equipment [6]. Extrusion-based AM (EAM) presents an alternative production technique that can be a relatively low cost [7] and straightforward to operate [8], with the capacity to manufacture complicated geometrical components [9]. The EAM is described as "the process of selectively dispensing material through a nozzle or orifice" [1]. Thermoplastics, short fiber reinforced thermoplastics, metals, technical ceramics, cermets, and hard metals [10], hybrid materials with comparable melting temperatures [11], and reinforced composites such as metal/polymer composites [12–15] can all be manufactured by EAM procedures. There is no waste of raw materials in EAM processes, and they are the best AM techniques for printing material combinations with homogeneous microstructure [16]. The manufacture of parts with acceptable characteristics, particularly metallic parts, is a significant challenge in this technique.

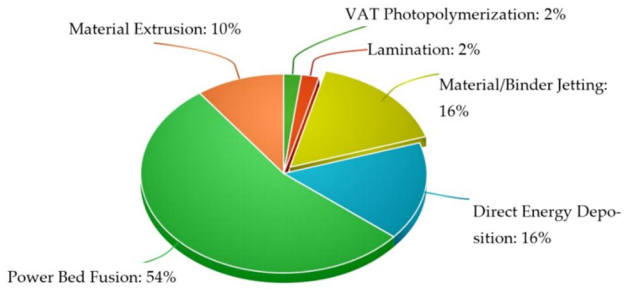

Fig. 1 Metal AM Market in 2020 [17]

The three primary metal EAM technologies are as follows: 1- direct ink writing (DIW), also referred to as robocasting or 3D gel-printing [18], 2- Semi-solid metal extrusion and deposition (SSMED), and 3- metal FDM. DIW is a metal extrusion-based method recently used to 3D print metallic components, especially porous titanium scaffolds (see, e.g. [19, 20]). This method fabricates components by extruding a paste or ink (a mixture of binder and metallic powder) through a small nozzle. The SSMED technique involves the layer-by-layer deposition of a metallic wire to create a metallic component. The wire must be heated to a mushy state and then semi-solidly extruded on the platform [4]. Metal FDM is used throughout this review article to refer to any techniques that utilize the procedure depicted in Fig. 2 to manufacture the parts. Thus, the initial stage in the metal FDM process is to produce a feedstock composed of binder and metallic powder. This feedstock can be manufactured as rods [21–23], filaments, or pellets. Accordingly, layer-wise deposition of the material is accomplished using plunger-based, pinch feed, or screw-based mechanisms, respectively [7]. The final metallic component is ready after posttreatment (including debinding and sintering steps). However, the method described here has been referred to as SDS (shaping, debinding, and sintering) [16, 24], BMD (bound metal deposition) [25], ADAM (atomic diffusion AM) [26], FDMet (fused deposition of metals) [27, 28], and MF3 (metal fused filament fabrication) [29]. These disparate names result from minor

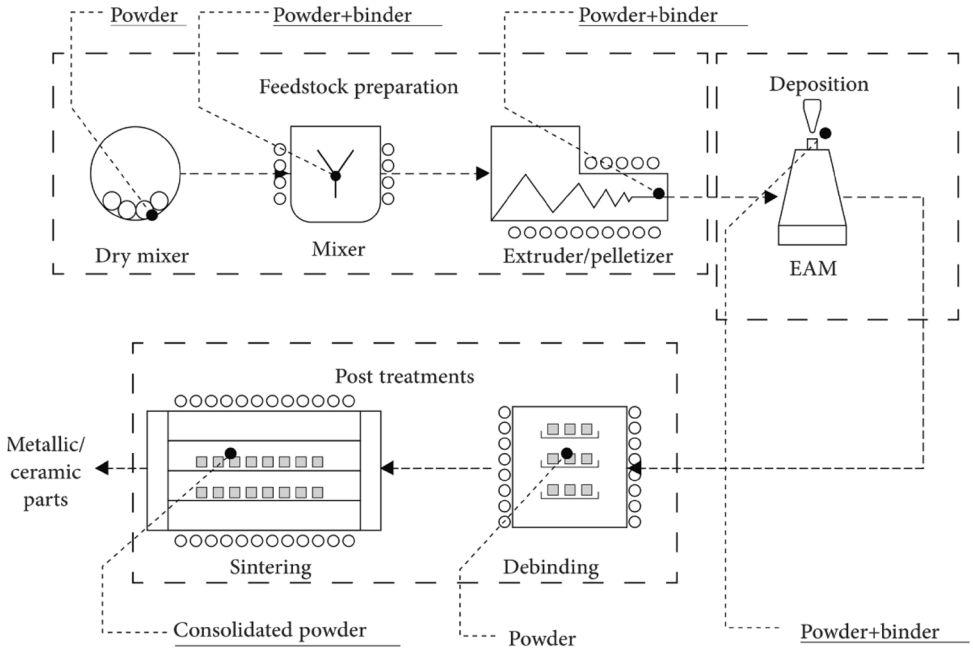

Fig. 2 Schematic of EAM process stages for manufacturing of metals and ceramics [10]

variations in the deposition technique utilized or corporations' monopoly on specific trademarks. One might also argue that referring to all metal EAM techniques that operate following Fig. 2 as metal FDM is erroneous. It does, however, contribute to the simplicity of the discussions and the manuscript's focus on the primary phases represented in this figure.

Although EAM is a low-cost technique that consumes less energy than SLM, it creates parts with lower density and mechanical properties [30]. Metal FDM powders and binders have a limited technological grasp. It could be stated that metal AM marketing information is limited, and the available information is comparable to the metal injection molding (MIM) marketing information about three decades ago [31]. Metal FDM has numerous similarities to BJ and MIM in various ways [32]. MIM is a widely used injection-based technique well suited to manufacturing tiny, accurate parts with complicated geometrical requirements. As a result, it is suggested to employ BJ and MIM technical data and standards for metal FDM, such as information for binders and powders, and so on. Although there are minor differences, for example, the amount of the binder in metal FDM is higher than in MIM technology to improve printability. Furthermore, producing MIM's green part utilizing metal FDM or BJ techniques lowers costs for single and small batch production [32].

This review aims to explore the metal FDM technique and its parameters. The various steps of this process will be covered, including shaping (preparation of feedstock and filament and 3D printing), debinding, and sintering (as illustrated in Fig. 2). Additionally, the mechanical and microstructural characteristics of the parts will be discussed, and the influence of process parameters on these attributes.

This review article is divided into six sections. Section 2 describes the shaping stage, which entails the preparation of feedstock and filament and the 3D printing of a green component. Section 3 discusses the green part's posttreatment (debinding and sintering). Section 4 explains the mechanical and microstructural properties of metal FDM parts and how they are affected by the process parameters. Section 5 discusses the use of finite element simulation in the analysis of metal FDM processes. Finally, Sect. 6 addresses the gaps and challenges and the areas for more study.

2 Shaping

Shaping is the initial stage of SDS processes. It consists of two steps: (1) preparing feedstock and filament (dry mixing of base metal powder with a suitable binder, mixing the powder/binder mixture at a temperature between the melting point and degradation temperature of the binder, and finally extrusion of feedstock in the form of granules or filament under appropriate shear stress), and (2) printing of a green component.

2.1 Feedstock preparation

The source material provided to the metal FDM is referred to as feedstock [1]. Three steps must be considered throughout the feedstock preparation stage: powder characterization, compounding of powder and binder, and filament manufacturing [33]. A polymeric-based binder and sinterable metal-based powder are utilized in the feedstock of metal FDM [34]. The binder is a multi-material component used to form and sustain the structure of powder-based parts [7]. Creating a binder composition that can offer flexibility and strength to filaments and green components is crucial in preparing feedstock [24]. Binder melting and degradation temperature points are two critical parameters that influence feedstock preparation, printing, and debinding circumstances. The values of these thermal parameters are shown in Table 1 for the components of a binder system used to manufacture a MIM feedstock. 60% of the feedstock is SS 316L powder. The feedstock mixing temperature should be adjusted higher than the maximum melting point (e.g., 165 °C for polypropylene) but lower than the lowest degradation temperature of the binder components (e.g., 270 °C for RWL) [35].

The shear viscosity of EAM feedstocks is the most critical element in their characterization [36]. Both powder and binder affect the thermal conductivity, heat capacitance, as well as regulating the maximum shear rate and other printing factors [37]. Like the MIM method, using a low viscosity binder can prevent powder segregation in the production of micro components [38]. Other features and criteria influenced by the binder system include maximum powder content, the strength of the green part, and properties of the final product after posttreatment [39]. The low melting temperature, high capability to wet the powder

Table 1 Components of a MIM feedstock's binder and their thermal properties [35]

Binder	Fraction in binder	Density (g/cm^3)	Melting temperature (°C)	Degradation temperature range (°C)
Polypropylene	0.5 (6.9 g)	0.90	165	350–470
Restaurant waste lipids (RWL) derivatives	0.5 (6.9 g)	0.90	50	270–360

particles, readily removed in posttreatment, be environmentally friendly are some of the properties of a suitable binder [40].

SS 316L powder and the powder and binder in the fractured section of the feedstock pellet are shown in Fig. 3. Embemould K83 (a commercial water-soluble binder) is used as a binder [9]. According to this figure, the SS 316L particles are adequately covered with the binder, and the feedstock has a relatively complete homogeneous structure. Table 2 shows a variety of binder systems that have been employed in various EAM process investigations. Because the usage of polymeric binder pollutes the atmosphere during the debinding process, eco-friendly materials such as PLA can be used [41].

The amount of base metal powder ranges from 50 to 60% by volume [10, 29]. Any change in powder content causes various shrinkage values and changes in green and final product characteristics. Particle size and powder production technique are two critical factors are studied by many researchers [31, 42]. Park et al. [42] showed that particle sizes substantially impact the densification behavior of printed components. Smaller particle size reduces feed supply viscosity and solid volume content [43]. The powder used in MIM and BJ is commonly generated utilizing water and gas atomization, which are relatively less expensive methods [44].

Because of the high-quality spherical particles generated by gas atomization, this method is preferred [60]. Metal is

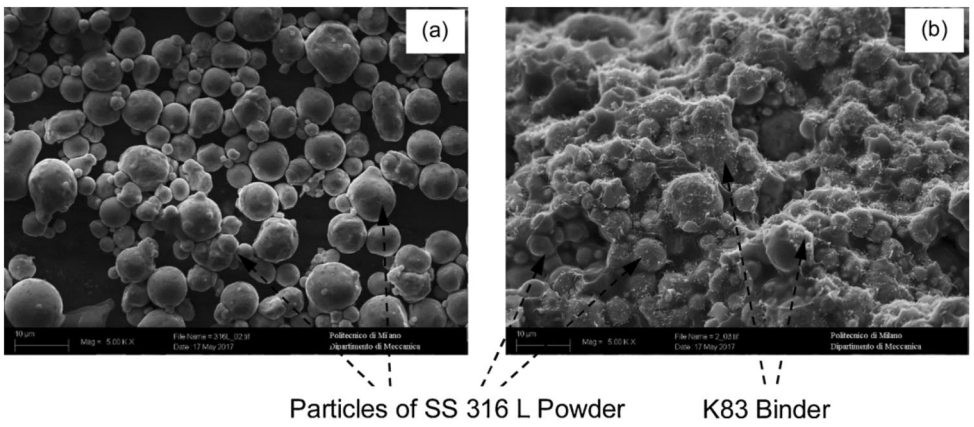

Fig. 3 Scanning electron microscopy (SEM) images of (**a**) SS 316L powder and (**b**) fractured section of a feedstock pellet [9]

Table 2 Binder systems utilized in different studies of metal EAM

Metal	Particle size µm	Solid loading vol%	Binder system	Ref.
Copper	12–81	65	Paraffin wax, low-density polyethylene, stearic acid	[45]
AISI 630	–	79	Water-soluble polyethylene glycol	[46]
Bronze	10–40	87	Polylactic acid (PLA)	[47]
Ti6Al4V	45	66	Methylcellulose, stearic acid	[48]
Silver	0.05	above 50 wt.%	Poly-4-vinyl phenol	[49]
SS 316L	–	60	Paraffin wax, high-density polyethylene, acetic acid-vinyl acetate copolymer, stearic acid	[50]
	9.93–90.84	63	Water-soluble Embemould K83 binder	[36]
	8.8	50, 54, 63	Water-soluble Embemould K83 binder	[51]
	10	60	Organic binder composed of Polyoxymethylene, paraffin wax	[27]
	30–50	88 wt.%	Polyformaldehyde and additives such as polypropylene, dioctyl phthalate, dibutyl phthalate, and ZnO	[52]
SS 17-4PH	4.2–28.2	55	Grafted polyolefin, a thermoplastic elastomer	[53]
	4.2–28.2	55	A soft and flexible thermoplastic elastomer (TPE) and polyolefin-based backbone and a commercially available compatibilizer	[54]
	4.2–28.2	55	A TPE with a grafted polyolefin	[55]
Copper	0.5	90 wt.%	Paraffin wax	[56]
	1	90 wt.%	Paraffin wax	[57]
	2–20	93.5 wt.%	Paraffin wax, Polyethylene glycol	[58]
	25, 106	50, 55, 60, 65 wt.%	Polyvinyl carboxy polymer, polyvinyl alcohol	[59]

frequently melted first, then atomized in a dedicated furnace under protected environment or vacuum conditions [44]. Plasma atomization, centrifugal atomization, mechanical attrition and alloying, melt spinning, rotating electrode technique, and various chemical processes are other powder production methods [61]. In certain circumstances, powder with very tiny particle sizes (0.1–10 µm and 0.2–20 µm particle sizes, respectively) might be generated using procedures such as chemical reduction and thermal decomposition [62]. However, while utilizing a powder with small particle sizes and an excellent spherical shape enhances the properties of the printed object, it considerably increases the cost of the powder.

Before combining the powder and binder, the powder particles were pre-dried at a high temperature (> 100 °C) for a few hours to eliminate moisture [34]. The powder characteristics are affected by the powder's base material, particle size and shape, specific surface area, and chemical composition [7]. Moreover, powder properties are influenced by solid loading, interparticulate friction, extrusion flow, and form stability during postprocessing [7]. The uniformity of powder dispersion in feedstock and filament is a crucial characteristic [63]. This quality influences printed objects' mechanical properties and density. The homogeneous distribution of powder in feedstock affects the material's rheological behavior and can aid in retaining forms during posttreatment [63].

Metals such as copper, SS 17-4PH, and SS 316L have been employed in numerous recent metal FDM studies. As one of the most studied metals in EAM, SS 316L is gaining increasing importance for researchers. This is due to the numerous advantages of SS 316L, including superior mechanical properties, good weldability and formability, and high corrosion and oxidation resistance. Furthermore, SS 316L has been widely used in military, medical, and other industries [64]. One of the first and best commercial SS 316L filaments was manufactured by BASF (UltraFuse 316LX), which consisted of a polymer matrix with dispersed 88 wt.% SS 316L particles with sizes ranging from 30 to 50 µm [52]. Markforged also created commercial filaments for the SS 17-4PH [10]. The development of commercial filaments can significantly lower production costs while also simplifying the manufacturing process [65]. Desktop Metal Inc (that names their technique-bound metal deposition) and Markforged Inc (that calls their process atomic diffusion AM (ADAM)) are two businesses located in the United States that are working in the metal EAM sector [66].

2.2 3D-printing of a green component

The printing process involves depositing filaments or pellets manufactured in the preceding step layer-by-layer through a small nozzle [67]. At this point, the 3D-printed part is referred to as a green part. In metal FDM, two printing methods are available:

1. Continuous printing from extruded granules; this technique is low-cost, and it is appropriate for research laboratory applications. The EFeSTO machine, shown in Fig. 4, is the first metal FDM 3D printer based on MIM extruder technology [68]. The extruder system is stationary in this machine, whereas the deposition plate is moved using a linear delta system.
2. Filament-based printing: this technology is suitable for commercial applications and is utilized by well-known firms such as Markforged, Desktop Metal, and BASF. SEM images of an SS 17-4PH green part produced by Markforged's ADAM process are shown in Fig. 5. As seen in this figure, the rasters are compacted and interdiffused. On the other hand, as illustrated in Fig. 5 (b), the rasters are dry and lack a distinct polymeric matrix between the particles, making the 17-4 PH green samples excessively brittle [69].

Several studies have demonstrated that printing parameters such as raster angle (see Fig. 6), build orientation (see Table 3), the thickness of layers (see Fig. 7), and infill percentage impact the properties of the products. The orientation of the printed samples influences their load-bearing

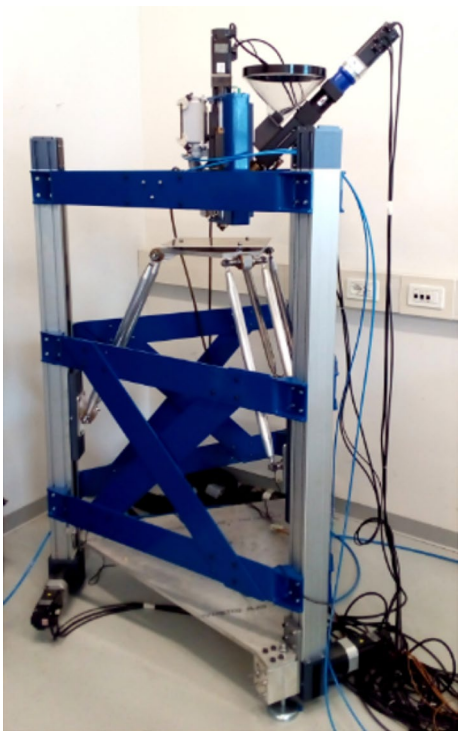

Fig. 4 The first 3D printer developed for metal FDM [68]

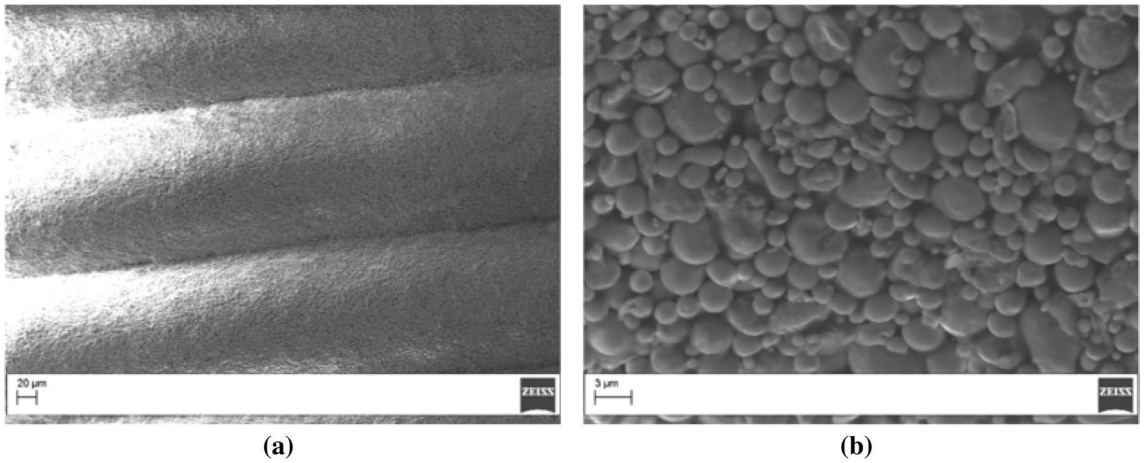

Fig. 5 SEM images of green part made of SS 17-4PH Markforged filament in different contour magnifications (**a**) 500×, and (**b**) 6000×[69]

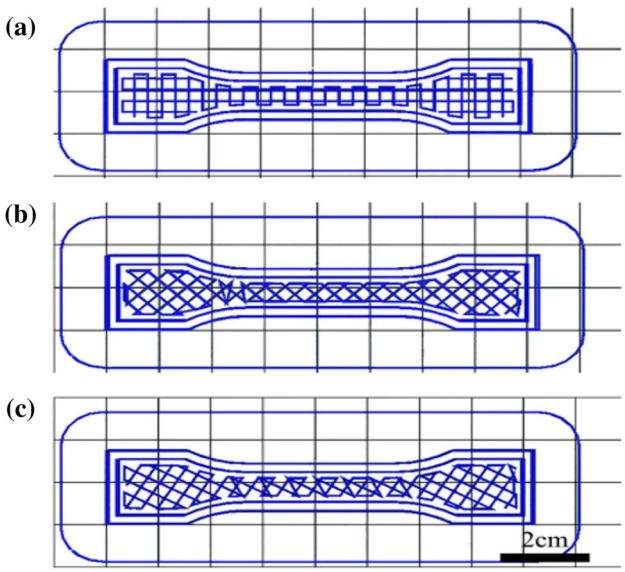

Fig. 6 Different raster angles in FDM printing of copper [45]

area. As a result, as seen in Table 3, flatwise samples exhibited superior tensile characteristics. Not only does layer thickness impact the mechanical properties of components, but it also has a significant effect on the surface quality, as demonstrated in Fig. 7. According to Ren et al. [45], the ultimate tensile strength of green samples was influenced by the printing parameters in the following order: the infill degree > raster angle > layer thickness. The form and size of the extrusion nozzle are significant factors that affect the amount of extrusion pressure and the filament diameter. Some studies look at filament characteristics, including bending and tensile strength [32].

As previously said, several companies, such as Markforged and Desktop Metal, supply important technological data, machines, and equipment in metal FDM. Thus, many studies compare their achieved findings with the technical data sheets of these companies (see Table 3). BASF, Markforged, and Desktop metal filaments (for example, "Ultrafuse 316LX" (BASF)) have been utilized in many research, and the influence of printing parameters on component characteristics has been examined [71], as seen in Table 3.

Green parts experience significant shrinking throughout the postprocessing phases (see, for example, Fig. 8). This phenomenon should be taken into account from the design phase [8]. In many EAM methods, the printed green sample must be connected to a support, which aids in the preservation of the part's form, displacement, and stability during the whole process from printing to post-sintering, particularly for surfaces with angles less than 45° (from the horizon)

Table 3 Comparison of tensile properties for the sintered parts with the technical data sheet provided by BASF company [69]

Material	Building orientation	Yield strength (MPa)	Tensile Strength (MPa)	Tensile Modulus (GPa)	Strain at Break (%)
SS 316L	Flatwise	148.01 ± 4.50	443.90 ± 5.87	157.24 ± 4.50	43.33 ± 2.53
SS 316L	Upright	113.75 ± 13.42	206.27 ± 80.11	117.31 ± 1.94	13.35 ± 6.59
SS 316L*	Flatwise	251	561	–	53
SS 316L*	Upright	234	521	–	36

*This data was extracted from the technical data sheet released by the producer (BASF for the SS 316L)

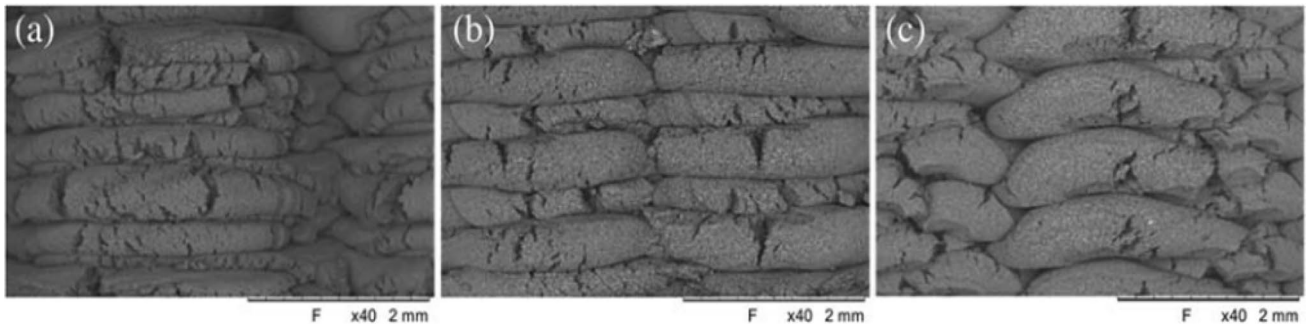

Fig. 7 SEM images of 3D-printed SS 316L samples, with different layer thicknesses (**a**) 0.3 mm, (**b**) 0.4 mm, and (**c**) 0.5 mm [70]

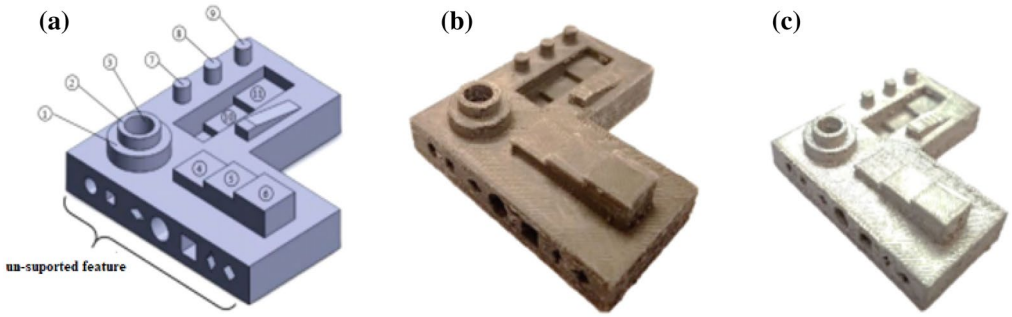

Fig. 8 **a** CAD model of a sample part, **b** green part, and **c** the final part after shrinkage due to thermal treatment [30]

[60]. The usage of proper support and its requirements is complicated and must be done with care. It is uncommon to find information on the support material and its removal in metal FDM. However, in the commercial metal FDM 3D printers of Markforged and Desktop Metal incorporation, a ceramic layer between the raft/support and the main part is printed. This ceramic layer disintegrates during the sintering process, which facilitates raft/support removal.

3 Posttreatment

The final part after posttreatment is referred to as a brown part [21]. The following sections cover two essential posttreatment procedures, debinding, and sintering, as well as their most important parameters and specifications. In terms of method and equipment, metal FDM debinding and sintering are comparable to MIM and BJ processes; however, several process parameters and the output are different.

3.1 Debinding

Debinding eliminates the majority of the binder material in the green part. This process is influenced by two factors: (1) the kind of debinding (solvent, thermal [72], catalytic [52, 73], or combination of these [66, 74]), and (2) the thermal cycle of the debinding process. Compared to solvent and catalytic debinding, thermal debinding is relatively slow [69] and easy to regulate [75]. The solvent debinding provides a transport channel for removing reminded binder during thermal debinding [58]. Temperature is a critical component in the debinding stage and must be precisely regulated. Therefore, as shown in Fig. 9, during solvent debinding, a controlled thermal cycle with moderate temperature changes should be selected.

Because of the binder volume loss, shrinkage, changes in weight, and size of the green part emerge. As shown in Fig. 10, the influence of the extrusion velocity (V_e) on the weight change (ΔW) is insignificant. The average ΔW value obtained after solvent debinding is approximately 3.5% percent; likewise, the average ΔW value obtained after thermal debinding and sintering is about 6.5% and 7.6%, respectively [28]. To maintain the component's form and minimize thermal stress and considerable weight reduction rates, the rate of temperature decline/increase in time must be slow enough [28].

Wall thickness variations and distortions caused by thermal processing should be considered, particularly in components with varying wall thicknesses. Additionally, numerical simulation can aid in estimating and

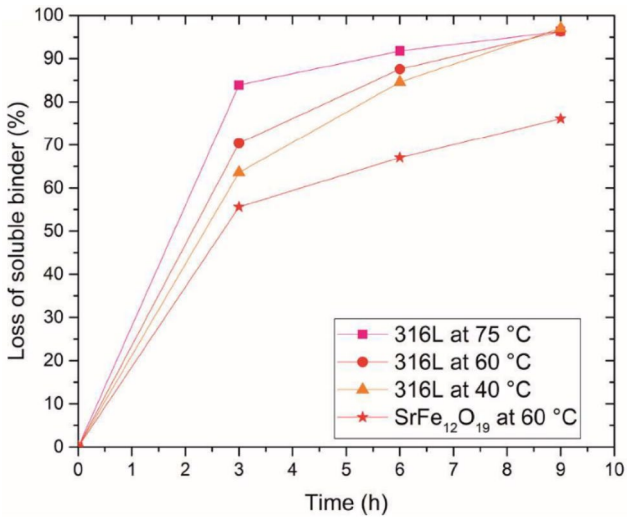

Fig. 9 Percentage of mass loss during solvent extraction for the parts made of SS 316L and strontium ferrite ($Fe_{12}O_{19}Sr$) [76]

compensating for shrinkage during multi-material post-treatment [15].

Most debinding processes employ two successive phases, solvent extraction and thermal debinding, and three significant stages occur in debinding: 1- diffusion of solvent, 2-dissolution of the soluble part of binder, and 3- diffusion from the inside to the outside for the remaining quantity of binder [34]. The following is a list of the various components of a binder system, along with their corresponding elimination conditions during posttreatment [66]:

1. The main binder component (50–90 volume percent of the entire binder system); during solvent debinding, this component of the binder system is eliminated.
2. The backbone (0–50 volume percent of the entire binder system); before sintering, the backbone that is used to hold the form of the green part is thermally removed.
3. Additives (0–10 volume percent of the entire binder system); they include dispersant agents, stabilizers, and compatibilizers.

However, if a one-step thermal debinding method is utilized, the binder system's constituents will be thermally removed. Even though the purpose of the debinding step is to remove the binder, in a multi-component binder system, the primary component may be eliminated early. Still, the second portion of the binder (with a very little quantity) retains the part form until the sintering stage, after which it can be removed at high temperatures during sintering [77].

3.2 Sintering

Atomic diffusion between metal powder particles happens with this thermal postprocessing treatment [77]. At this step, conditions for obtaining near-total density are achieved using high temperatures (below the melting point of the metal) [78]. Full density is not attained due to the presence of tiny residual micro-porosities [46]. Three significant parameters influence the ultimate outcomes of sintering: (1) temperature, (2) time, and (3) furnace atmosphere. Utilizing a gradual and regulated temperature cycle is critical in sintering, as it is in debinding. Thermal debinding and sintering are continuous operations that occur one after the other and usually in the same furnace.

The sintering cycle depicted in Fig. 11 exhibits two gradual temperature rises. The leftover binder is devolatilized and eliminated during the first hours of sintering. Following that, the metal particles fuse, and the metallic microstructure develops from the part's outside to its inside [79].

Residual stress at grain surfaces and stress between grains increase as temperatures increasse toward completing the sintering cycle [80]. As seen in Fig. 12, necking between metal particles occurs as time and temperature rise. As sintering continues, the size of the neck rises, and the dimension of the pore decreases [60].

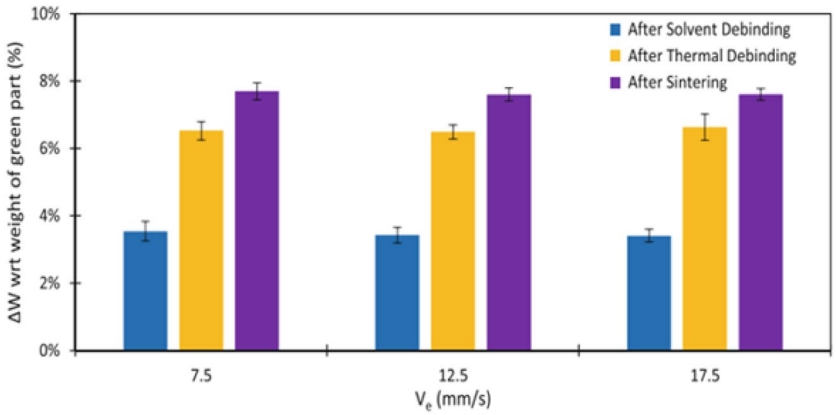

Fig. 10 Weight changes during posttreatment of SS 316L parts manufactured at various extrusion velocities, V_e [28]

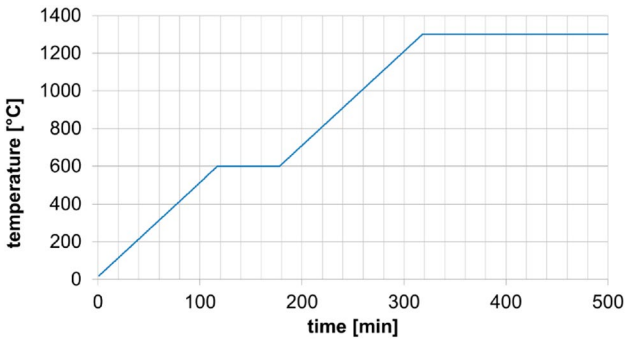

Fig. 11 Sintering cycle for SS 17-4PH part [79]

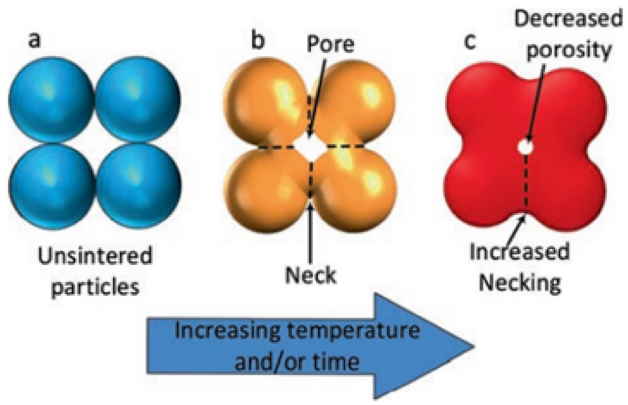

Fig. 12 Joining of base metal powder particles during sintering [60]

The most appropriate sintering environment should be chosen to achieve the best characteristics, lowest costs, and highest production rates. For example, according to Raza et al. [72], the rate of debinding for SS 316L in a vacuum furnace is faster than in a hydrogen atmosphere. Furnaces with a vacuum or inert gas environment should be used for sintering to avoid thermal oxidation of the powders and, as a result, the final component [81, 82].

Various atmospheres have different effects on microstructure. As depicted in Fig. 13, a thick, elongated film forms at the grain boundaries during M2 high-speed steel samples' sintering at 1200 °C, indicating over-sintering. However, a homogenous structure was obtained when the samples were sintered in an N_2–H_2 atmosphere. The sintering environment also affects the chemical composition of sintered samples [83]. According to Dourandish and Simchi [84], sintering zirconia ceramic and SS 430L in a vacuum result in lower mismatch strain than sintering in an argon environment.

Microwave sintering uses less energy and takes less time than traditional sintering [85], and in certain circumstances results in better mechanical characteristics [86]. Microwave sintering, for example, causes high densities in 434L steels but reduced density in SS 316L. It reduces hardness, strength, and ductility in both austenitic and austenitic-ferritic stainless steel [87]. Microwave sintering produces fully recrystallized microstructures with fractionally larger grain sizes in SS 316L [88]. The effect of various critical parameters on sintered component characteristics is depicted in Figs. 14 and 15. These figures show that sintering at an optimum temperature for a more extended period and a slower temperature change yields better results for the component's microstructure [89]. Using homogeneous feedstocks and filaments aids in obtaining a uniform and isotropic shrinkage during the debinding and sintering [7].

4 Mechanical and microstructural properties

The ASTM F3122-14 standard guideline is concerned with the mechanical characteristics of metallic parts created using AM technology [90]. Table 4 illustrates the elements of the metal FDM process that impact the properties of the

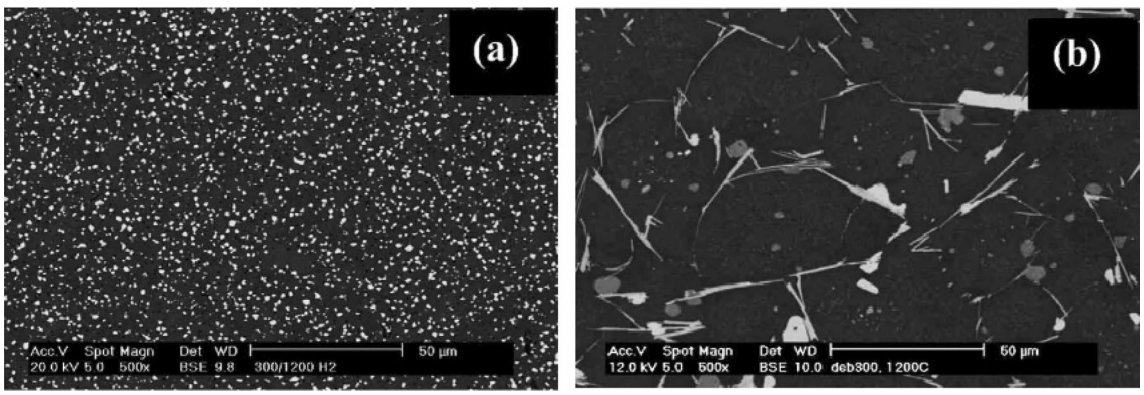

Fig. 13 SEM images of M2 high speed steel samples sintered in 1200 °C, **a** in N_2–H_2 atmosphere, and **b** vacuum [83]

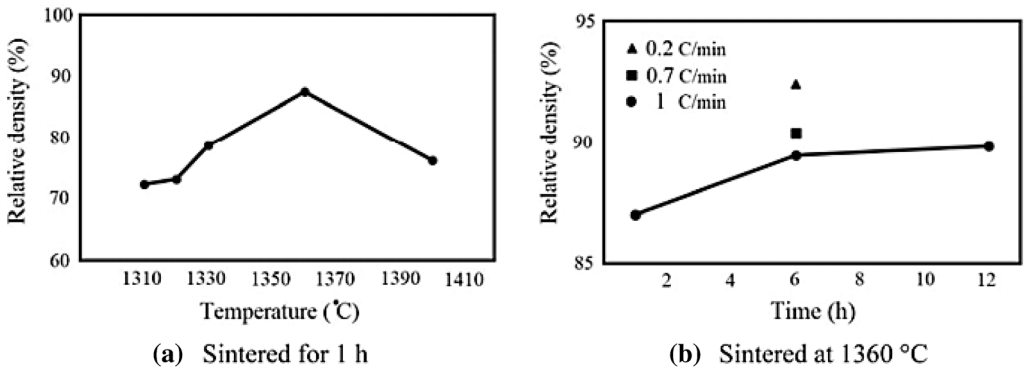

Fig. 14 Influence of sintering temperature and time on the relative density [89]

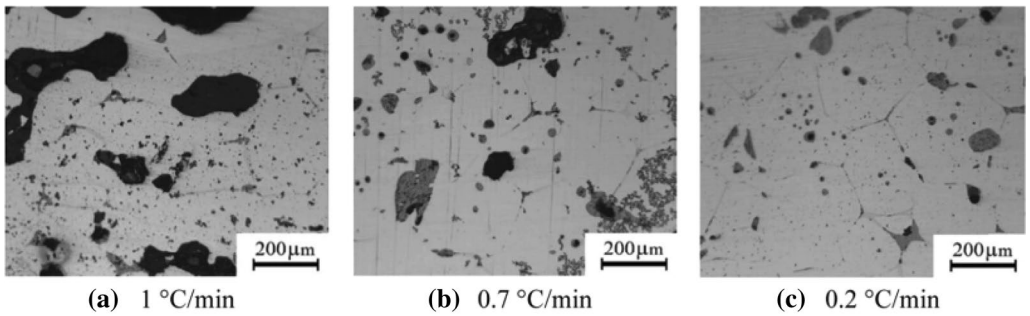

Fig. 15 Influence of various debinding rates on the microstructure of SS 316L samples sintered at 1360 °C for 6 h [89]

Table 4 Main factors affect the properties of parts produced using metal FDM processes

Metal FDM steps	Parameters
Design	Dimensional design, part's shape complexity
Characterization of feedstock constitutes	Size, shape, and chemical composition of powder particles, powder drying conditions, granulometry of the powder, binder type and composition
Extrusion and feedstock preparation	Rotational speed, pressure and temperature of the extruder, extruder's nozzle temperature and diameter, granule viscosity, the volume fraction of the metal powder in feedstock, shear stress in preparation of the feedstock, bending and tensile strength of the filament
Print	Bed temperature, cooling rate after deposition, printing speed, build orientation, infill type, raster angle, adhesion of layers, layer's height and width, melting and degradation temperatures of the filament
Debinding and sintering	Cycle time and temperature, atmosphere, and pressure of furnace, residual carbon, toxic metal ions, nitrogen, or other elements of the sintered part, type and quality of equipment and furnaces

3D-printed components. Although the impacts of many of these factors have been demonstrated in numerous studies, additional studies on metal FDM procedures with more details and more accurate modeling should be done in the future to get superior mechanical characteristics.

The characteristics of SS 316L parts generated by different methods were compared in Table 5. This table shows that metal FDM products have relatively poor mechanical characteristics compared to SLM or traditionally manufactured components. For example, the ultimate tensile strength of SS 316L parts manufactured using metal FDM was 465 MPa, approximately 72% of the SLM sample's ultimate tensile strength (648 MPa). One major cause is the presence of metallurgical flaws such as porosities. Minimal porosity is a common and accepted defect in AM metallic components. Additionally, the following factors contribute to the poor mechanical properties of 3D-printed metallic parts: rapid temperature fluctuations, capillary forces, and gravity without applying external pressure in the binding mechanisms, shrinkage in a posttreatment, material supply

Table 5 Tensile properties of SS 316L alloy produced using different processes

Process	Yield strength (MPa)	Ultimate tensile strength (MPa)	Elongation at break (%)	Young's modulus (GPa)
Metal FDM [30]	167	465	31	152
SLM [30]	541	648	30	320
Wrought [93]	205	515	60	193

shortage, and absence of deposition (melting, fusing, or binding) [60, 91]. Despite this, Markforged claims that the density of their metal components manufactured from SS 17-4PH (using Metal X 3D printer) is more than the density of MIM's product [92].

It must be remembered that the final dimensions and mechanical characteristics are affected by parameters such as excessive shrinkage during the debinding process and shrinkage and distortion during the sintering process. Table 6 depicts the influence of printing parameters on part shrinkage in different orientations. As this table indicates, the flatwise specimens exhibit a linear shrinkage of roughly 20% in the XY plane, whereas a higher shrinkage (25.20%) was measured in the Z direction. The samples printed upright demonstrate more anisotropic behavior with values ranging from 8.57 to 20.70%. This anisotropic behavior is controlled by the impact of gravity on the metal component during the sintering process.

Powder particle size, together with sintering temperature, affects the final component characteristics and microstructure [78]. As indicated in Table 7, raising the sintering temperature to 1395 °C and utilizing SS 316L powder with a particle size of 31 µm resulted in the highest tensile strength and elongation and the highest density for the final part [94]. Table 8 shows the effect of the vital printing settings on the ultimate tensile strength of copper. The optimum combination of the parameters mentioned in this table is (45°/45°), 2 mm, and 80%, respectively. Figure 16 depicts the impacts of various multi-metal component printing techniques. Material infill levels have enhanced compressive strength while not influencing printed component shrinking [71]. Mechanical characteristics are affected by printing orientation; for example, vertically printed components have lower tensile strength [71].

Table 7 Characteristics of sintered parts made from powders with varying particle sizes sintered at different temperatures [94]

Powder particle size (µm)	Sintering temperature (°C)	Final density (%) ± 0.1%	Max. strength (MPa) ± 6%	Elongation (%) ± 5%
31	1255	81.0	309	21.3
	1355	85.2	388	35.5
	1365	90.9	437	52.1
	1395	98.0	518	61.9
20 – 53	1415	81.8	243	25.4
	1432	88.2	310	29.9

Table 8 Effect of printing parameters on ultimate tensile strength [45]

No	Raster angle (°)	Layer thickness (mm)	Infill percentage (%)	Ultimate tensile strength (MPa)
1	0/90	1.6	80	5.08 ± 0.45
2	0/90	1.8	70	5.57 ± 0.61
3	0/90	2.0	60	4.21 ± 0.29
4	45/ – 45	1.6	70	5.66 ± 0.51
5	45/ – 45	1.8	60	3.35 ± 0.28
6	45/ – 45	2.0	80	6.73 ± 0.87
7	60/ – 30	1.6	60	5.17 ± 0.49
8	60/ – 30	1.8	80	5.13 ± 0.44
9	60/ – 30	2.0	70	5.12 ± 0.38

Some factors, such as layer thickness and extrusion temperature, have an optimal level. Small layer height, for example, might result in poor forming quality (squeeze effect), whereas high layer height can cause the preceding layer to sink (sinking effect) [56]. Increased extrusion velocity results in increased porosity in SS 316L sintered parts, as demonstrated in Fig. 17.

In the cross-section of the green part shown in Fig. 18, the appropriate distribution of SS 17-4PH particles (brighter spots) and certain flaws as a result of poor setting

Table 6 Dimensional comparison of green and sintered SS 316L parts [69]

Build Orientation	Printing direction	Green part (mm)	Sintered part (mm)	Shrinkage (%)
Flatwise	*Y*	22.80	19.04	19.73
	Z	3.75	3.02	25.20
	X	137.98	115.25	19.72
Upright	*X*	22.80	19.35	17.81
	Y	3.78	3.48	8.57
	Z	137.98	114.31	20.70

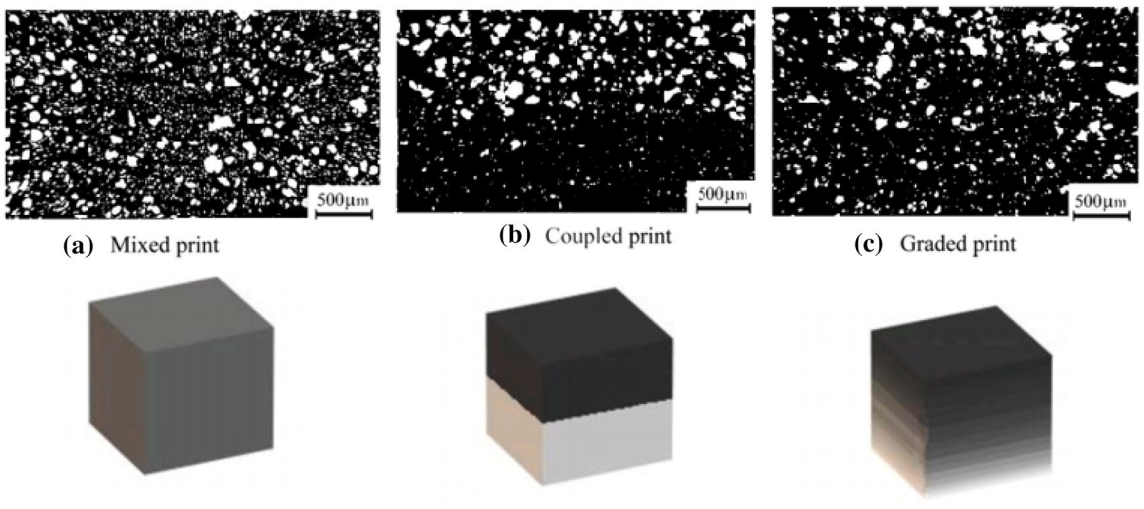

Fig. 16 Schematic representations and optical microscope images of three types of multi-metal parts (high carbon iron and SS 316L), **a** mixed (50–50%), **b** coupled (100–100%), and **c** functionally graded (0–100%) samples [89]

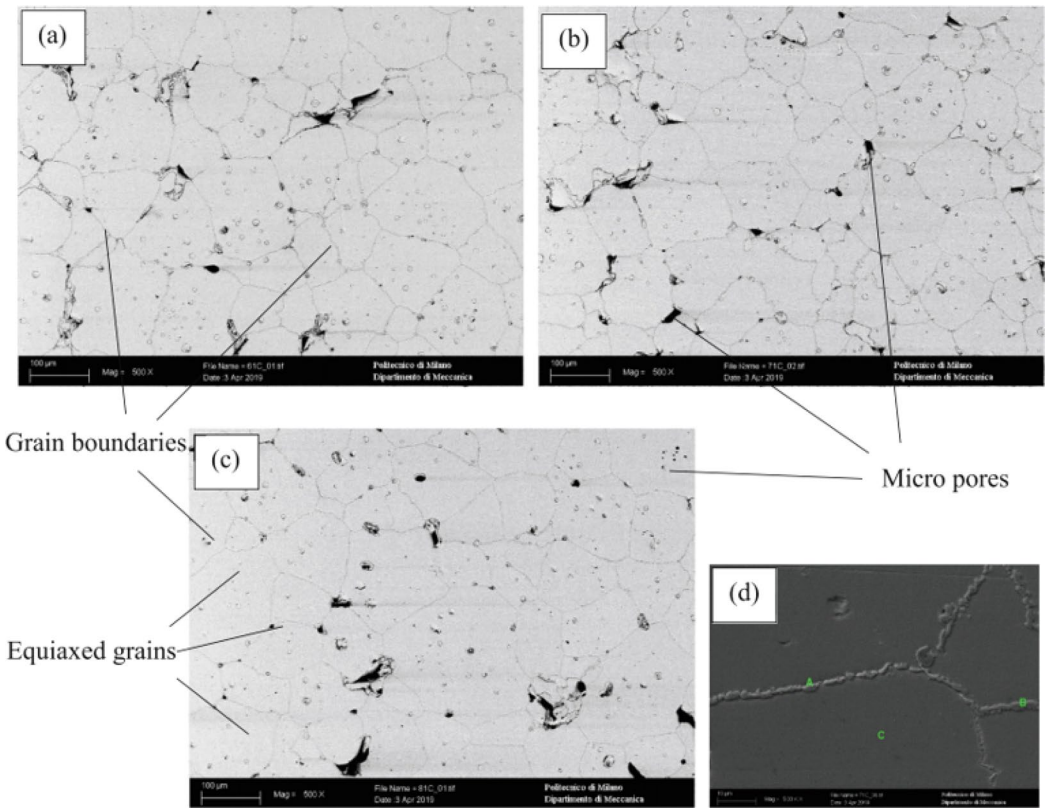

Fig. 17 Microstructure of sintered SS 316L parts printed at **a** 7.5 mm/s, **b** 12.5 mm/s, **c** 17.5 mm/s, extrusion velocity, and **d** elemental analysis [28]

during printing (for example, tiny spaces between the layers) are visible [54].

After sintering and debinding, the chemical composition of components must be monitored. The characteristics of sintered parts, such as surface morphology, are affected by residual carbon content during debinding [72]. Carbon content substantially impacts densification rate and has a reducing function in sintering [95]. The initial carbon

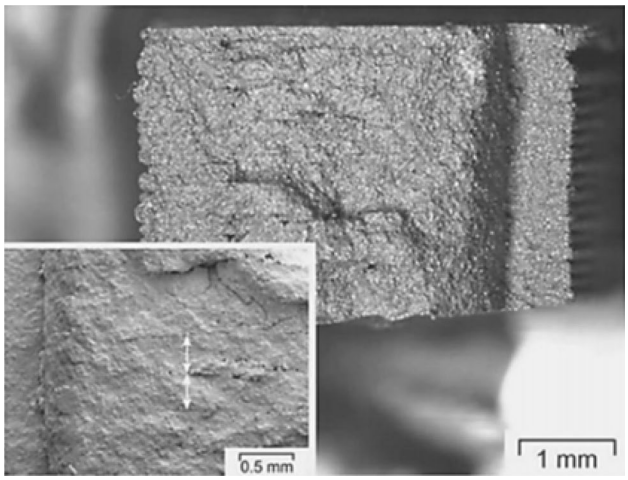

Fig. 18 Fracture section of SS 17-4PH part [54]

Table 9 Carbon content in sintered SS 316L parts at different atmospheres (ASTM E1019) [72]

Sintering atmosphere	Carbon %
Vacuum	0.00636
H_2	1.4955
H_2 & N_2 mixture	1.3215
N_2	0.1392

concentration in the powder and the residual carbon content after debinding should be very low, similar to MIM, as this might decrease the final part's corrosion performance [96]. As shown in Table 9, the sintering environment influenced the quantity of this chemical element in SS 316L. The best results, i.e., the lowest carbon content (0.0063%), were obtained by sintering in a vacuum [72]. Furthermore, the nitrogen content of sintered components drops progressively as the sintering temperature rises, increasing relative density when nitrogen pressure is precisely controlled [97]. Although microstructural analysis after sintering has been examined in some publications, however, it can be claimed that there is not enough reliable information on this subject.

Many aspects in the whole production stages impact the quantity of porosity as the significant consequence of flaws and weak mechanical characteristics. Choosing the best cycle for temperature and heating rate, as shown in Figs. 19 and 20, has a high impact on the amount of porosity and, as a result, mechanical characteristics. According to Fig. 19, increasing the sintering temperature from 1340 °C to 1360 °C resulted in increased sample density and decreased residual porosity. However, Fig. 20 indicates that raising the sintering temperature does not necessarily result in a rise in density. On the other hand, it is necessary to attain an optimal sintering temperature.

Posttreatment of metal AM parts lowers production defects and improves microstructure and mechanical characteristics [3]. Chemical surface treatment methods, for example, have been used to enhance fatigue performance and smooth the surface of AM components, as well as heat treatments at high temperatures to relieve residual stresses [3]. As shown in Fig. 21, with surfaces inclined at various degrees, the mean roughness (Ra) changes. Furthermore, this figure indicates that sintered samples have better roughness than green parts, and vertical and horizontal surfaces have superior roughness.

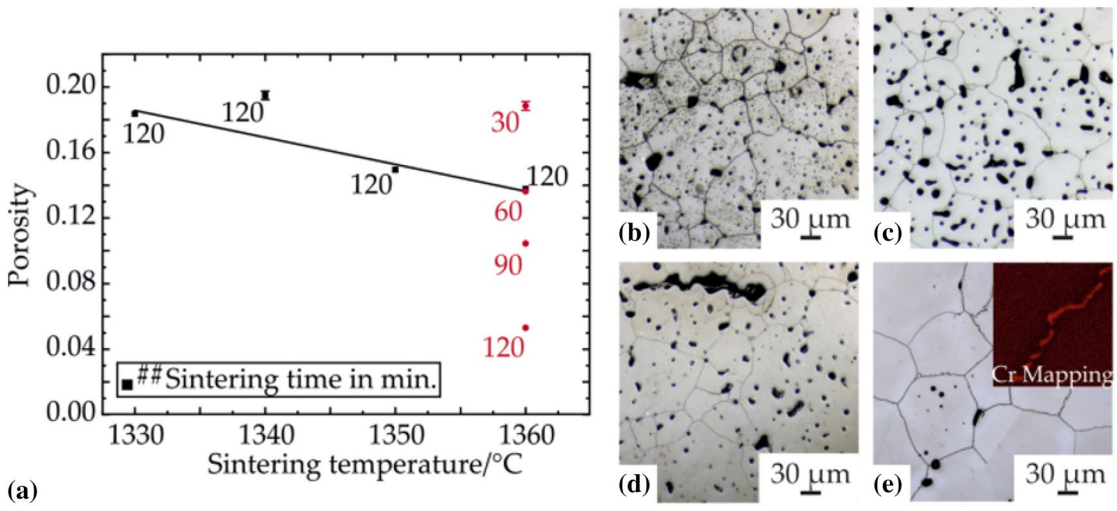

Fig. 19 **a** Porosity in SS 316L samples for different sintering temperatures and times (heating rate 0.3 °C/min), and microstructural images for sintering at (**b**) 1340 °C, **c** 1350 °C, **d** 1360 °C, and **e** 1360 °C (heating rate of 0.2 °C/min and sintering time of 120 min) [65]

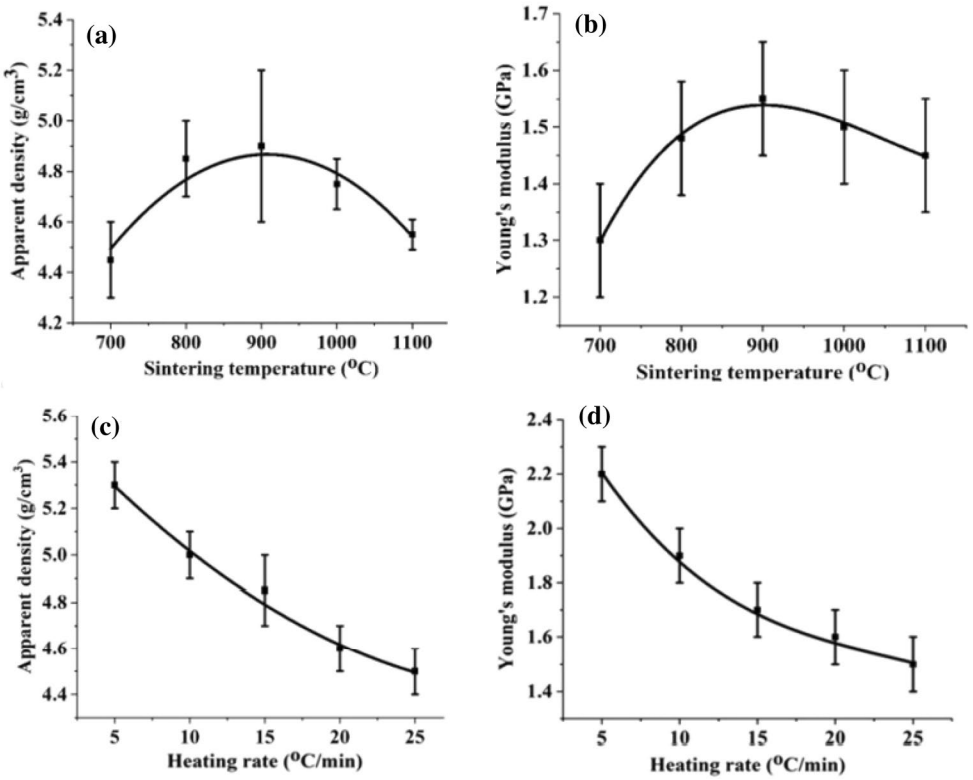

Fig. 20 Effect of heating rate and sintering temperature on apparent density and Young's modulus of porous iron scaffolds [98]

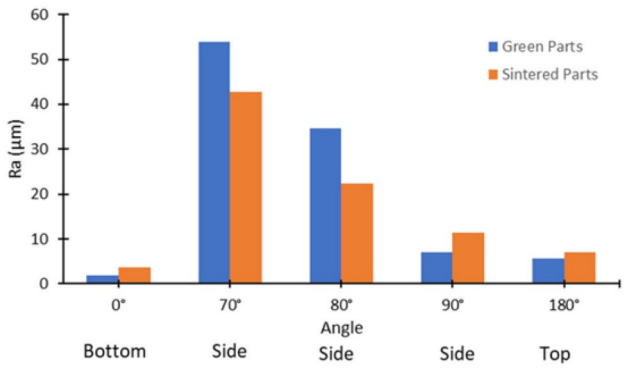

Fig. 21 Comparison of surface roughness of green and sintered samples [10]

5 Finite element modeling (FEM)

The use of FEM can aid in the correct design and calculation of controlled modifications and predict the form and distortion of green and final components. It eliminates or significantly lowers the need for significant and costly testing equipment, machinery, and materials. FEM research in metal FDM is insufficient. Furthermore, developing specialized software for predicting final component size, residual stresses, and estimating ultimate mechanical characteristics for various metals would aid in advancing metal FDM.

Figure 22 shows the results of a thermomechanical finite element analysis for predicting shrinkage, warpage, and internal stresses during the sintering process, providing information about possible weak areas of the part [8]. Figure 23 shows the results of a debinding numerical simulation for a staircase as another example. According to this figure, orientations 1 and 3 are the best choices for debinding. In these orientations, all elements experience stress values less than predefined critical stresses. On the other hand, the debinding of the part in orientations 2, 4, and 6 will cause failure due to excessive tensile and compressive stresses. Additionally, the simulation results show that there are very few critical elements in orientation 5. Since these elements surpass the critical compression stress limit, the part will fail during sintering.

Using GOM Inspect software, Ait-Mansour et al. [74] estimated shrinkage percentages in sintered components manufactured of BASF Ultrafuse 316LX. Furthermore, printing accuracy and dimensional variations in metal FDM-fabricated components may be evaluated and predicted using neural networks and other algorithms [99].

6 Research gaps and challenges

For the future development of metal FDM and its industrialization, a complete cycle in manufacturing technology must first be considered, with ample and easily accessible

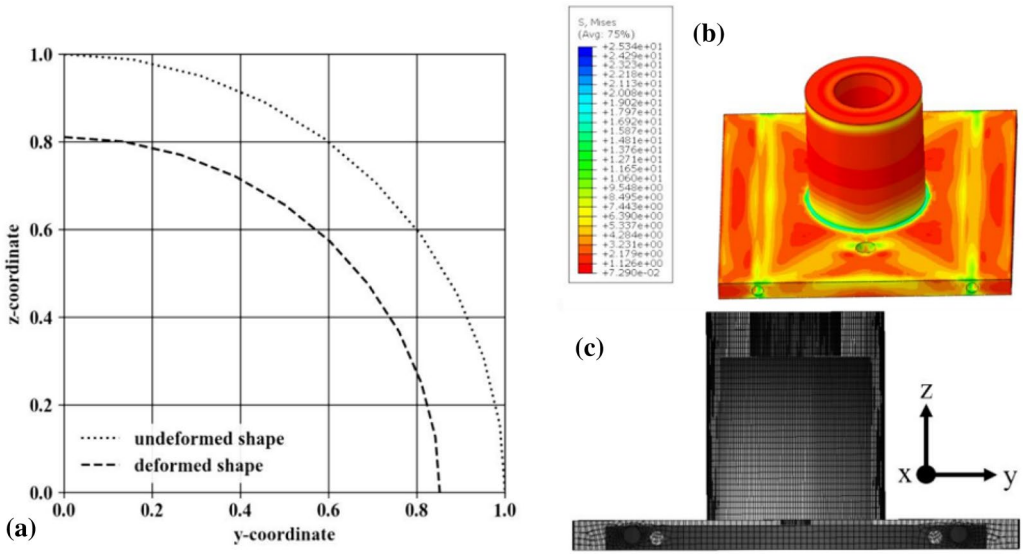

Fig. 22 Finite element simulation of a 3D printed metal part, (**a**) ovalization of the circular holes due to shrinkage, (**b**) stress distribution, and (**c**) overlay plots of the original and deformed parts [8]

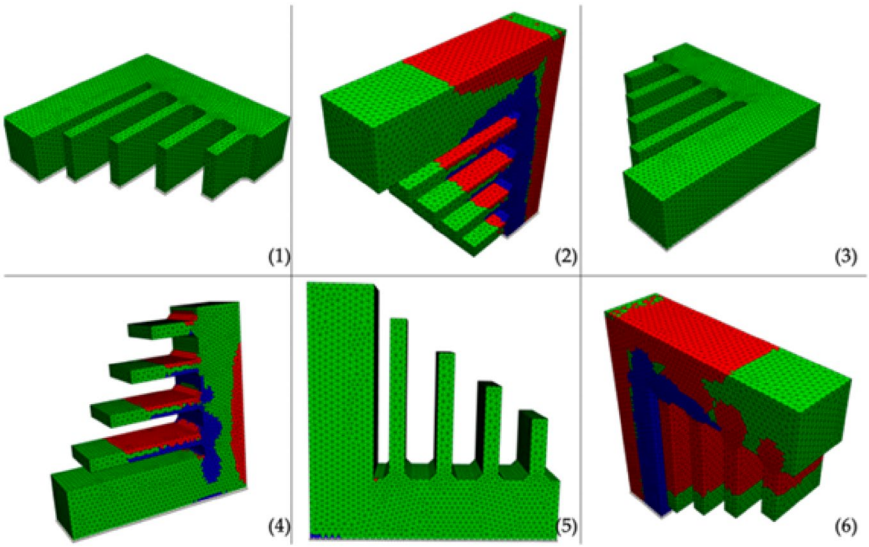

Fig. 23 Failure plots for simulation of the debinding process (red areas show failure due to tension, and the blue regions indicate failure due to compression) [73]

materials and equipment for production. Then, flaws in product quality must be eliminated. Optimization of technology in terms of cost, quality, and accuracy should be considered in the second stage. It might be claimed that metal FDM's initial stage is still unfinished, with many tough questions and difficulties to be answered. The following are some of these questions and difficulties:

1. Establish a sufficient level of control and analysis of metallurgical characteristics and microstructure.
2. Increased mechanical characteristics, such as tensile strength, for a broader range of applications
3. Development of low-cost commercial materials such as filaments, binders, and powders are easy to come by.
4. To achieve a broad range of capabilities and applicability for unique situations such as complicated forms, thin-walled components, and high-precision dimensions.
5. Providing metal FDM and subtractive manufacturing hybrid methods with significant advantages in manufacturing components with unique engineering characteristics.
6. Compared to other metal AM technologies, major companies in this sector, such as Markforged and Desktop Metal, have not made adequate and significant development.
7. Numerical simulation research in metal FDM is insufficient. Moreover, the development of specialized software for predicting the final component's size, residual

stresses, and predicting ultimate mechanical characteristics for various metals would assist in the progress of metal FDM.

However, the significant advantages of this technology, such as its ease of use and relatively low cost of production, and capacity to manufacture large parts, have sparked interest among corporations and researchers to enhance metal FDM technology.

Acknowledgements The authors wish to express their gratitude to Dr. Hasan Abdoos (Department of Nanotechnology, Faculty of New Sciences and Technologies, Semnan University, Semnan) for reading the manuscript and providing helpful suggestions for article improvement. The authors also would like to thank the numerous researchers whose work has been represented in this review paper.

Funding No funding was received for conducting this study.

Availability of data and materials Not applicable.

Code availability Not applicable.

Declarations

Conflict of interest The authors have no conflicts of interest to declare that are relevant to the content of this article.

Ethical approval Not applicable because this article does not contain any studies with human or animal subjects.

Consent to participate Not applicable.

Consent to publish Not applicable.

References

1. ISO/ASTM52900-15 (2015) Standard terminology for additive manufacturing—general principles—terminology, ASTM International, West Conshohocken, PA. www.astm.org
2. Shirazi SFS et al (2015) A review on powder-based additive manufacturing for tissue engineering: Selective laser sintering and inkjet 3D printing. Sci Technol Adv Mater 16:033502
3. Zadpoor AA (2018) Frontiers of additively manufactured metallic materials. Materials 11:1–10
4. Jabbari A, Abrinia K (2018) A metal additive manufacturing method: semi-solid metal extrusion and deposition. Int J Adv Manuf Technol 94:3819–3828
5. Pack RC, Compton BG (2021) Material extrusion additive manufacturing of metal powder-based inks enabled by Carrageenan rheology modifier. Adv Eng Mater 23:2000880
6. Roshchupkin SI, Golovin VI, Kolesov AG, Tarakhovskiy AY (2020) Extruder for the production of metal-polymer filament for additive technologies. IOP Conf Ser Mater Sci Eng 971:022009
7. Rane K, Strano M (2019) A comprehensive review of extrusion-based additive manufacturing processes for rapid production of metallic and ceramic parts. Adv Manuf 7:155–173
8. Rosnitschek T, Hueter F, Alber-Laukant B (2020) FEM-based modelling of elastic properties and anisotropic sinter Shrinkage of metal EAM. Int J Simul Model 19:197–208
9. Strano M, Rane K, Briatico Vangosa F, Di Landro L (2019) Extrusion of metal powder-polymer mixtures: Melt rheology and process stability. J Mater Process Technol 273:116250
10. Strano M, Rane K, Farid MA, Mussi V, Zaragoza V, Monno M (2021) Extrusion-based additive manufacturing of forming and molding tools,". Int J Adv Manuf Technol. https://doi.org/10.1007/s00170-021-07162-8
11. Chávez FA, Quiñonez PA, Roberson DA (2019) Hybrid metal/thermoplastic composites for FDM-type additive manufacturing. J Thermoplast Comp Mater. https://doi.org/10.1177/0892705719864150
12. Çevik Ü, Kam M (2020) A review study on mechanical properties of obtained products by FDM method and metal/polymer composite filament production. J Nanomater. https://doi.org/10.1155/2020/6187149
13. Boparai KS, Singh R, Singh H (2016) Experimental investigations for development of Nylon6-Al-Al2O3 alternative FDM filament. Rapid Prototyp J 22:217–224
14. Fu X, Zhang X, Huang Z (2021) Axial crushing of Nylon and Al/Nylon hybrid tubes by FDM 3D printing. Compos Struct 256:113055
15. Scheithauer U, Slawik T, Schwarzer E, Richter HJ, Moritz T, Michaelis A (2015) Additive manufacturing of metal-ceramic-composites by thermoplastic 3D-printing (3DTP). J Ceram Sci Technol 6:125–132
16. Lengauer W et al. (2018) Preparation and properties of extrusion-based 3D-printed hardmetal and cermet parts. Euro PM 2018 Congress and Exhibition
17. Vafadar A, Guzzomi F, Rassau A, Hayward K (2021) Advances in metal additive manufacturing: a review of common processes, industrial applications, and current challenges. Appl Sci 11:1–33
18. Ren X, Shao H, Lin T, Zheng H (2016) 3D gel-printing-An additive manufacturing method for producing complex shape parts. Mater Des 101:80–87
19. Li JP, de Wijn JR, Van Blitterswijk CA, de Groot K (2006) Porous Ti6Al4V scaffold directly fabricating by rapid prototyping: preparation and in vitro experiment. Biomaterials 27(8):1223–1235
20. Elsayed H et al (2019) "Direct ink writing of porous titanium (Ti6Al4V) lattice structures. Mater Sci Eng 103:109794
21. Nurhudan AI, Supriadi S, Whulanza Y, Saragih AS (2021) Additive manufacturing of metallic based on extrusion process: a review. J Manuf Process 66:228–237
22. Wohlers T (2017) Desktop metal: a rising star of metal AM targets speed, cost and high-volume production. Metal AM: 89–92
23. Campbell I, Wohlers T (2017) Markforged: taking a different approach to metal additive manufacturing
24. Kukla C, Gonzalez-Gutierrez J, Hampel S, Burkhardt C, Holzer C (2017) The SDS process: a viable way for the production of metal parts. 11th International Conference on Industrial Tools and Advanced Processing Technologies
25. Watson A, Belding J, Ellis BD (2020) Characterization of 17–4 PH processed via bound metal deposition (BMD). TMS 2020 149th Annual Meeting & Exhibition Supplemental Proceedings. Springer, Cham, Switzerland. pp 205–216
26. Galati M, Minetola P (2019) Analysis of density, roughness, and accuracy of the atomic diffusion additive manufacturing (ADAM) process for metal parts. Materials 12(24):4122
27. Kurose T et al (2020) Influence of the layer directions on the properties of 316l stainless steel parts fabricated through fused deposition of metals. Materials 13:2493
28. Hassan W, Farid MA, Tosi A, Rane K, Strano M (2021) The effect of printing parameters on sintered properties of extrusion-based

additively manufactured stainless steel 316L parts. Int J Adv Manuf Technol 114(9):3057–3067
29. Singh P, Balla VK, Tofangchi A, Atre SV, Kate KH (2020) Printability studies of Ti-6Al-4V by metal fused filament fabrication (MF3). Int J Refract Metals Hard Mater 91:15249
30. Gong H, Snelling D, Kardel K, Carrano A (2019) Comparison of stainless steel 316L parts made by FDM- and SLM-based additive manufacturing processes. JOM 71:880–885
31. Capus J (2020) Making steel powders for PM and AM. Metal Powder Rep 75:148–150
32. Korotchenko AY, Khilkov DE, Tverskoy MV, Khilkova AA (2020) Use of additive technologies for metal injection molding. Eng Solid Mech 8:143–150
33. Wu G, Langrana NA, Sadanji R, Danforth S (2002) Solid freeform fabrication of metal components using fused deposition of metals. Mater Des 23:97–105
34. Kukla C, Cano S, Kaylani D, Schuschnigg S, Holzer C, Gonzalez-Gutierrez J (2019) Debinding behaviour of feedstock for material extrusion additive manufacturing of zirconia. Powder Met 62:196–204
35. Amin AM, Ibrahim MHI, Asmawi R, Mustaffa N, Hashim MY (2017) Thermal debinding and sintering of water atomised SS316L metal injection moulding process. IOP Conf Series Mater Sci Eng 226:12155
36. Rane K, Farid MA, Hassan W, Strano M (2021) Effect of printing parameters on mechanical properties of extrusion-based additively manufactured ceramic parts. Ceram Int 47:12189–12198
37. Ahn S, Park SJ, Lee S, Atre SV, German RM (2009) Effect of powders and binders on material properties and molding parameters in iron and stainless steel powder injection molding process. Powder Technol 193:162–169
38. Quinard C, Barriere T, Gelin JC (2009) Development and property identification of 316L stainless steel feedstock for PIM and μPIM. Powder Technol 190:123–128
39. Momeni V, Alaei MH, Askari A, Rahimi AH, Nekouee K (2020) Effect of the fraction of steel 4605 powder in the load in injection molding with the use of a polymer-based binder. Metal Sci Heat Treat 61:777–781
40. Virdhian S, Doloksaribu M, Supriadi S, Balfas NM, Suharno B, Shieddieque AD (2020) Characterization of 17–4 PH stainless steel metal injection molding feedstock using mixing torque data. IOP Conf Ser Mater Sci Eng 980:20
41. Toropkov N, Lerner M, Mironov E (2019) Feedstock investigation based on SAE 316L steel bimodal powders and PLA/PMMA for injection molding: an experimental study. AIP Conf Proc 2167:20367
42. Park DY et al (2017) Investigation of powder size effects on sintering of powder injection moulded 17–4PH stainless steel. Powder Metal 60:139–148
43. Rane K et al. (2018) Rapid production of hollow SS316 profiles by extrusion based additive manufacturing. AIP Conference Proceedings 1960
44. Kassym K, Perveen A (2019) Atomization processes of metal powders for 3D printing. Mater Today Proc 26:1727–1733
45. Ren L et al (2017) Process parameter optimization of extrusion-based 3D metal printing utilizing PW-LDPE-SA binder system. Materials 10:305
46. Annoni M, Giberti H, Strano M (2016) Feasibility study of an extrusion-based direct metal additive manufacturing technique. Procedia Manuf 5:916–927
47. Lu Z, Ayeni OI, Yang X, Park HY, Jung YG, Zhang J (2020) Microstructure and phase analysis of 3D-printed components using bronze metal filament. J Mater Eng Perform 29:1650–1656
48. Li JP, De Wijn JR, Van Blitterswijk CA, De Groot K (2006) Porous Ti6Al4V scaffold directly fabricating by rapid prototyping: preparation and in vitro experiment. Biomaterials 27:1223–1235
49. Kang H, Kitsomboonloha R, Jang J, Subramanian V (2012) High-performance printed transistors realized using femtoliter gravure-printed sub-10 μm metallic nanoparticle patterns and highly uniform polymer dielectric and semiconductor layers. Adv Mater 24:3065–3069
50. Li J, Xie Z, Zhang X, Zeng Q, Liu H (2010) Study of metal powder extrusion and accumulating rapid prototyping. Key Eng Mater 443:81–86
51. Rane K, Di Landro L, Strano M (2019) Processability of SS316L powder—binder mixtures for vertical extrusion and deposition on table tests. Powder Technol 345:553–562
52. Liu B, Wang Y, Lin Z, Zhang T (2020) Creating metal parts by fused deposition modeling and sintering. Mater Lett 263:127252
53. Gonzalez-Gutierrez J, Arbeiter F, Schlauf T, Kukla C, Holzer C (2019) Tensile properties of sintered 17–4PH stainless steel fabricated by material extrusion additive manufacturing. Mater Lett 248:165–168
54. Gonzalez-Gutierrez J, Guráň R, Spoerk M, Holzer C, Godec D, Kukla C (2018) 3D printing conditions determination for feedstock used in fused filament fabrication (FFF) of 17-4PH stainless steel parts. Metalurgija 57:117–120
55. Godec D, Cano S, Holzer C, Gonzalez-Gutierrez J (2020) Optimization of the 3D printing parameters for tensile properties of specimens produced by fused filament fabrication of 17–4PH stainless steel. Materials 13:774
56. Yan X, Hao L, Xiong W, Tang D (2017) Research on influencing factors and its optimization of metal powder injection molding without mold via an innovative 3D printing method. RSC Adv 7:55232–55239
57. Yan X, Wang C, Xiong W, Hou T, Hao L, Tang D (2018) Thermal debinding mass transfer mechanism and dynamics of copper green parts fabricated by an innovative 3D printing method. RSC Adv 8:10355–10360
58. Singh G, Missiaen JM, Bouvard D, Chaix JM (2021) Copper additive manufacturing using MIM feedstock: adjustment of printing, debinding, and sintering parameters for processing dense and defectless parts. Int J Adv Manuf Technol 115:449–462
59. Hong S, Sanchez C, Du H, Kim N (2015) Fabrication of 3D printed metal structures by use of high-viscosity cu paste and a screw extruder. J Electron Mater 44:836–841
60. Gibson I, Rosen D, Stucker B, Khorasani M (2021) Additive manufacturing technologies. Gewerbestrasse 11, 6330 Cham, Switzerland. 685
61. Antony LVM, Reddy RG (2003) Processes for production of high-purity metal powders. JOM 55:14–18
62. Miranda R (2013) Handbook of metal injection molding. Int J Environ Stud 70:165–165
63. Liu L, Loh NH, Tay BY, Tor SB, Murakoshi Y, Maeda R (2005) Mixing and characterisation of 316L stainless steel feedstock for micro powder injection molding. Mater Charact 54:230–238
64. Weston NS, Thomas B, Jackson M (2019) Processing metal powders via field assisted sintering technology (FAST): a critical review. Mater Sci Technol 35:1306–1328
65. Thompson Y, Gonzalez-Gutierrez J, Kukla C, Felfer P (2019) Fused filament fabrication, debinding and sintering as a low cost additive manufacturing method of 316L stainless steel. Addit Manuf 30:100861
66. Gonzalez-Gutierrez J, Cano S, Schuschnigg S, Kukla C, Sapkota J, Holzer C (2018) Additive manufacturing of metallic and ceramic components by the material extrusion of highly-filled polymers: a review and future perspectives. Materials 11:840
67. Rane K, Castelli K, Strano M (2019) Rapid surface quality assessment of green 3D printed metal-binder parts. J Manuf Process 38:290–297

68. Giberti H, Sbaglia L, Silvestri M (2017) Mechatronic design for an extrusion-based additive manufacturing machine. Machines 5:29
69. Tosto C, Tirillò J, Sarasini F, Cicala G (2021) Hybrid metal/polymer filaments for fused filament fabrication (FFF) to print metal parts. Appl Sci 11:1
70. Rane K, Barriere T, Strano M (2020) Role of elongational viscosity of feedstock in extrusion-based additive manufacturing of powder-binder mixtures. Int J Adv Manuf Technol 107:4389–4402
71. Ait-Mansour I, Kretzschmar N, Chekurov S, Salmi M, Rech J (2020) Design-dependent shrinkage compensation modeling and mechanical property targeting of metal FFF. Prog Addit Manuf 5:51–57
72. Raza MR et al (2017) Effects of debinding and sintering atmosphere on properties and corrosion resistance of powder injection molded 316 L—stainless steel. JSM 46:285–293
73. Rosnitschek T, Glamsch J, Lange C, Alber-Laukant B, Rieg F (2021) An automated open-source approach for debinding simulation in metal extrusion additive manufacturing. Designs 5:1–15
74. Parenti P, Cataldo S, Annoni M (2018) Shape deposition manufacturing of 316L parts via feedstock extrusion and green-state milling. Manuf Letters 18:6–11
75. Gong P, Yan X, Xiong W, Hao L, Tang D, Li Y (2020) Design of a debinding process for polymetallic material green parts fabricatedviametal paste injection 3D printing with dual nozzles. RSC Adv 10:18000–18007
76. Gonzalez-Gutierrez J, Godec D, Kukla C, Schlauf T, Burkhardt C, Holzer C (2017) Shaping, debinding and sintering of steel components via fused filament fabrication. 16th International Scientific Conference on Production Engineering—CIM2017; 99–104
77. Tuncer N, Bose A (2020) Solid-state metal additive manufacturing: a review. JOM 72:3090–3111
78. Mirzababaei S, Pasebani S (2019) A review on binder jet additive manufacturing of 316L stainless steel. J Manuf Mater Process 3:82
79. Lieberwirth C, Sarhan M, Seitz H (2018) Mechanical properties of stainless-steel structures fabricated by composite extrusion modelling. Metals 8(2):84
80. Zhang Y, Bai S, Riede M, Garratt E, Roch A (2020) A comprehensive study on fused filament fabrication of Ti-6Al-4V structures. Addit Manuf 34:101256
81. Cerejo F, Gatões D, Vieira MT (2021) Optimization of metallic powder filaments for additive manufacturing extrusion (MEX). Int J Adv Manuf Technol. https://doi.org/10.1007/s00170-021-07043-0
82. Ye H, Liu XY, Hong H (2008) Sintering of 17–4PH stainless steel feedstock for metal injection molding. Mater Lett 62:3334–3336
83. Várez A, Levenfeld B, Torralba JM, Matula G, Dobrzanski LA (2004) Sintering in different atmospheres of T15 and M2 high speed steels produced by a modified metal injection moulding process. Mater Sci Eng A 366:318–324
84. Dourandish M, Simchi A (2009) Study the sintering behavior of nanocrystalline 3Y-TZP/430L stainless-steel composite layers for co-powder injection molding. J Mater Sci 44(5):1264–1274
85. Olevsky EA, Dudina DV (2018) Field-assisted sintering: science and applications. Field-Assisted Sintering: Science and Applications. Gewerbestrasse 11, 6330 Cham, Switzerland. 1–425
86. Anklekar RM, Agrawal DK, Roy R (2001) Microwave sintering and mechanical properties of PM copper steel. Powder Metal 44:355–362
87. Panda SS, Singh V, Upadhyaya A, Agrawal D (2006) Sintering response of austenitic (316L) and ferritic (434L) stainless steel consolidated in conventional and microwave furnaces. Scripta Mater 54:2179–2183
88. Ertugrul O, Park HS, Onel K, Willert-Porada M (2014) Effect of particle size and heating rate in microwave sintering of 316L stainless steel. Powder Technol 253:703–709
89. Mousapour M, Salmi M, Klemettinen L, Partanen J (2021) Feasibility study of producing multi-metal parts by Fused Filament Fabrication (FFF) technique. J Manuf Process 67:438–446
90. ASTM F3122-14 (2014) Standard guide for evaluating mechanical properties of metal materials made via additive manufacturing processes, ASTM International, West Conshohocken. http://www.astm.org
91. Cooke S, Ahmadi K, Willerth S, Herring R (2020) Metal additive manufacturing: Technology, metallurgy and modelling. J Manuf Process 57:978–1003
92. Markforged (2020) Material datasheet 17-4 PH stainless steel: 1–2
93. ASM (2014) AISI Type 316L Stainless Steel ASM: 1–2
94. Verlee B, Dormal T, Lecomte-Beckers J (2012) Density and porosity control of sintered 316L stainless steel parts produced by additive manufacturing. Powder Metall 55(4):260–267
95. Lou JK et al (2020) Investigation of decarburization behaviour during the sintering of metal injection moulded 420 stainless steel. Metals 10:211
96. Torralba JM (2012) Metal injection molding (MIM) of stainless steel. In: Donald FH (ed) Woodhead Publishing, Handbook of Metal Injection Molding: 393–414
97. Shang F, Wang Z, Chen X, Ji Z, Ren S, Qu X (2021) UNS S32707 hyper-duplex stainless steel processed by powder injection molding and supersolidus liquid-phase sintering in nitrogen sintering atmosphere. Vacuum 184:109910
98. Mishra DK, Pandey PM (2020) Effect of sintering parameters on the microstructure and compressive mechanical properties of porous Fe scaffold fabricated using 3D printing and pressure less microwave sintering. Proc Inst Mech Eng C J Mech Eng Sci 234:4305–4320
99. Zhang Z, Femi-Oyetoro J, Fidan I, Ismail M, Allen M (2021) Prediction of dimensional changes of low-cost metal material extrusion fabricated parts using machine learning techniques. Metals 11:690